# Monazite in metasediments from Stensjöstrand: A pilot study

*Andreas Olsson*

**Dissertations in Geology at Lund University,**
**Bachelor's thesis, no. 358**
**(15 hp/ECTS credits)**

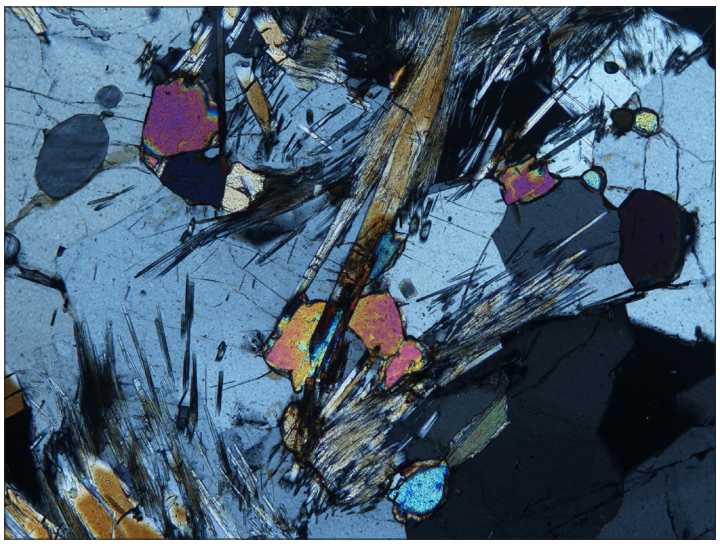

**Department of Geology**
**Lund University**
**2013**

# Monazite in metasediments from Stensjöstrand: A pilot study

Bachelor's thesis

Andreas Olsson

Department of Geology
Lund University
2013

# Contents



**Cover Picture:** Monazite in thin section. Photo Andreas Olsson.

# Monazite in metasediments from Stensjöstrand: A pilot study

ANDREAS OLSSON

Olsson, A., 2013: Monazite in metasediments from Stensjöstrand: A pilot study. *Dissertations in Geology at Lund University*, No. 358, 13 pp. 15 hp (15 ECTS credits) .

**Abstract:** Monazite is a Th-bearing REE phosphate mineral which is present in some igneous and metamorphic rocks. It is a useful mineral for determination of the metamorphic history and age of its host rock because clues to past mineral reactions can be seen in trace element zoning. Monazite has been found in metasediments in Stensjöstrand and thin sections have been made from rock samples to study the mineral. Thin sections 3c and 3b represent a migmatite gneiss with two different phases, mesosome and leucosome. The thin sections have been observed using polarization microscopy and two different types of monazite were discovered. The first type appears as small and oval or round crystals, often with distinct compositional domains and is found the leucosome. The second type appears as large, markedly irregular shaped crystals with indistinct compositional domains and is found the mesosome. The chemical compositions as well as the compositional domains of different monazite crystals and the main mineral assemblage have been analyzed using SEM-EDX. The results show a clear difference in mineral composition and texture between the leucosome and the mesosome. Minerals found in the leucosome are quartz, plagioclase, K-feldspar, zircon and small biotite, ilmenite and monazite crystals. Minerals found in the mesosome are sillimanite, quartz, plagioclase, K-feldspar, garnet, zircon, and large biotite (some of them containing symplectites), ilmenite, hematite and monazite crystals. BSE-images reveal exsolution textures in K-feldspar and ilmenite. Analytical results from different compositional domains of different monazite crystals were inconsistent and not completely accurate and could only be used to compare relative differences in chemical composition between crystals. The acual reason for the difference between the two types of monazite crystals is not certain. It is hypothesized that the difference is due to a difference in age between the two types and resorption of the large monazite crystals in the mesosome.

**Keywords:** Monazite, metasediments, Sveconorwegian orogen, Stensjöstrand, pilot study.

**Supervisor(s):** Charlotte Möller and Leif Johansson.

**Subject:** Bedrock geology.

*Andreas Olsson, Department of Geology, Lund University, Sölvegatan 12, SE-223 62 Lund, Sweden.*
*E-mail: marcus.andreas.olsson@live.se*

# Monazit i metasediment från Stensjöstrand: en pilotstudie

ANDREAS OLSSON

Olsson, A., 2013: Monazit i metasediment från Stensjöstrand: en pilotstudie. *Examensarbeten i geologi vid Lunds universitet*, Nr. 358, 13 sid. 15 hp.

**Sammanfattning:** Monazit är ett Ree– och Th-bärande fosfatmineral som förekommer i vissa magmatiska och metamorfa bergarter. Mineralet är användbart för datering av den metamorfa utvecklingen och kan bidra till att ytterligare karaktärisera metamorfosen i en bergart, detta genom att man undersöker zoneringar i kristallerna. Monazit har upptäckts i metasediment i Stensjöstrand och tunnslip har gjorts ifrån prover för att undersöka mineralet. Tunnslip 3c och 3b kommer ifrån en migmatitgnejs som har två skilda faser, mesosom och leukosom. Tunnslipen har studerats med polarisationsmikroskopi och två olika typer av monaziter har upptäckts. Den första typen är små och ovala eller runda, ofta med distinkt zonering, och de förekommer i leukosomen. Den andra typen har stora, påtagligt oregelbundet formade kristaller med otydlig zonering och de förekommer i mesosomen. Kemisk sammansättning och zonering i olika monazitkristaller och resterande mineralsällskap har analyserats med SEM-EDX. Resultaten visar en tydlig skillnad i mineralsammansättningen och texturer mellan leukosomen och mesosomen. Mineral som förekommer i leukosomen är kvarts, plagioklas, K-fältspat, zirkon och små biotit-, ilmenit- och monazitkristaller. Mineral som förekommer i mesosomen är sillimanit, kvarts, plagioklas, K-fältspat, granat, zirkon och stora biotit- (vissa har symplektit-inneslutningar), ilmenit-, hematit– och monazitkristaller. Back-scatterbilder visar avblandningar i både K-fältspat och ilmenit. Erhållna analysresultat från olika domäner i olika monazitkristaller är inkonsekventa och inte fullständigt korrekta och kunde endast användas för att jämföra relativa skillnader i de kemiska sammansättningarna mellan olika kristaller. Den faktiska orsaken till skillnaderna mellan de två olika typerna av moanzitkristallerna är inte säker. En hypotes är att orsaken till skillnaden är en skillnad i ålder mellan de två typerna och resorbtion av de de stora monazitkristallerna i mesosomen.

**Nyckelord:** Monazit, metasediment, Sveconorvegiska orogenesen, Stensjöstrand, pilotstudie.

*Andreas Olsson, Geologiska institutionen, Lunds universitet, Sölvegatan 12, 223 62 Lund, Sverige.*
*E-post: marcus.andreas.olsson@live.se*

# 1 Introduction

The purpose of the present study is to investigate the occurrence of a mineral called monazite in metasedimentary rocks from Stensjöstrand, Halland. Main questions were:

What information can be gained from the textures and overall mineral assemblage in the rock sample?

Is there any complexity in the monazite crystals?

Can an analysis of the mineral give insight to past metamorphic events that have affected the host rock?

The bedrock at Stensjöstrand, Halland, has been affected by high-grade metamorphism. The study has focused on two thin sections, 09SGC-3b and 09SGC-3c, of a rock sample of migmatite gneiss from the study area. The thin sections were first investigated using polarization microscopy. The main mineral assemblage and the overall texture were documented and also potential monazite crystals were located. As a second step the thin sections were investigated with scanning electron microscope linked with an energy-dispersive X-ray equipment (SEM-EDX). The chemical compositions of the minerals found in the thin sections were analyzed. The results are presented and further discussed below.

# 2 Geologic Setting

Stensjöstrand is located in the eastern part of the Sveconorwegian Province, in the Eastern Segment (Fig. 1) where the bedrock is characterized by high-grade metamorphism and dominated by migmatitic rocks. The high-grade metamorphism is a result of two orogenesis, the first being the Hallandian orogenesis at ca 1.44-1.42 Ga and the second being the Sveconorwegian continent-continent collision at ca 0.98-0.92 Ga. Foliation is regionally developed in this metamorphic province in both large and small scales. The metamorphic facies diagram (Fig. 2) illustrates the P-T relations required for the mineral assemblages in the Stensjöstrand area; high-pressure granulite and upper amphibolite facies.(Dean et al., 2008)

The investigated rocks at Stensjöstrand are pelitic metasediments, which have undergone high-grade metamorphism and partial melting and formed migmatitic gneisses consisting of two main parts: sillimanite-rich mesosome and granitic leucosome. Both parts are folded and of almost equal size and extent. The leucosome is granitic, has a red color and sugary texture while the mesosome is dark, mainly because of its biotite and opaque mineral content (Fig. 3A). The sillimanite-rich mesosome has a different erosion surface than the thick leucosomes, which locally is up to 2 dm wide (Fig. 3B). The mesosome is mostly light grey in color and has rounded erosions surfaces. The granitic leucosome is commonly parallel to the mesosome and folded. Equigranular leucosome pods which cut across the folds appear locally.

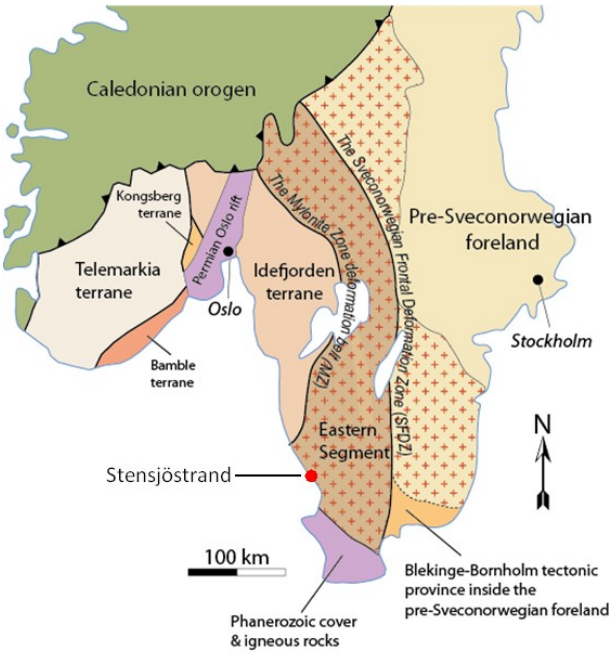


*Fig. 1.* The Sveconorwegian Province. Stensjöstrands approximate location is marked on the image. (J. Andersson & C. Möller, Unpublished. Modified after Möller et al., 2007)

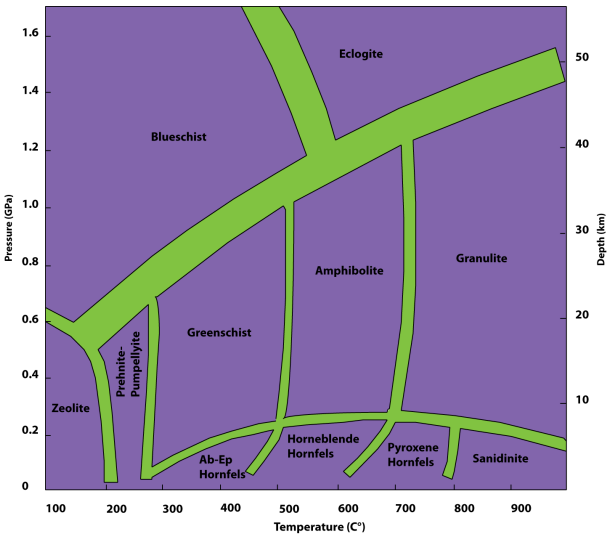


*Fig. 2.* Pressure, temperature and depth (PTD) diagram showing different metamorphic facies. (Modified after diagram from Winter, 2010)

# 3 Monazite

Monazite is a phosphate mineral of the formula $REEPO_4$ containing light rare earth elements (LREE). It has a monoclinic crystal system and its color can vary between yellow, brown and reddish brown. Commonly the crystals are very small (a few µm across); larger crystals are rare (Williams et al., 2007).

The LREE that are most commonly found in monazite are Ce, La, Nd and Y. Because REE have chemical similarities they often substitute one another;

therefore the chemical composition can vary between and within individual monazite crystals (BGS, 2011). Non-REE such as Th, Ca, Si, F, Cl and more rarely S can also substitute for the LREE found in monazite. The most common substitutions in monazite are:

$$P^{+5} + REE^{3+} \leftrightarrow Si^{4+} + Th^{4+}$$
$$2REE^{3+} \leftrightarrow Ca^{2+} + Th^{4+}$$

The first of these variations of monazite is known as huttonite and the second is known as cheralite (Williams et al., 2007). Due to the common occurrence of Th and U in monazite, sometimes enough to be of commercial interest, the mineral is radioactive. The radioactive elements produce Pb in the monazite crystal. The radioactivity can over a large period of time result in damage to the mineral crystal (Boatner, 2002).

Monazite appears as an accessory mineral in both alkaline igneous rocks and metamorphic rocks and can also originate from hydrothermal processes. It has been found concentrated in beach sands and streams as a detrital mineral (Deer et al., 1962). According to Spear & Pyle (2002) monazite is stable at and above greenschist facies in rocks of appropriate bulk composition.

Monazite is in the modern day used in science to study the age and metamorphic history of rocks and is commercially a source of REE, Th and U. Monazite dating utilizes Th/Pb, U/Pb or Pb/Pb ratios of individual spots of microdomains in situ within crystals (analysis within in its textural setting). Information about the reaction history in a metamorphic rock is retrieved from trace elements and trace element zoning in minerals (Spear and Pyle, 2002).

# 4 Analytical Methods

Several thin sections were available from rocks in the Stensjöstrand study area. Two thin sections, 09SGC-3b and 09SGC-3c were chosen for close investigation (Fig. 4). These two thin sections represent the sillimanite gneiss with red granitic leucosome shown in Figs. 3A & B. Both were studied with polarized light microscopy and thereafter carbon coated and investigated with scanning electron microscopy and energy-dispersive X-ray spectroscopy (SEM-EDX) at the Department of Geology, Lund University. The purpose was to examine the shape of the monazite crystals in different textural positions, their chemical composition and possible compositional zoning. The other minerals in the thin section were identified by polarized light microscopy and their chemical compositions analyzed by SEM-EDX. The SEM equipment is a Hitachi S-3400N equipped with an EDX and INCA software. During analysis, the voltage was set to 15 kV and the instrument was calibrated using a Co-standard. Natural and synthetic mineral standards were used for analysis of the main elements. Spot analysis was primarily used to identify the chemical composition of the different minerals in the thin sections.

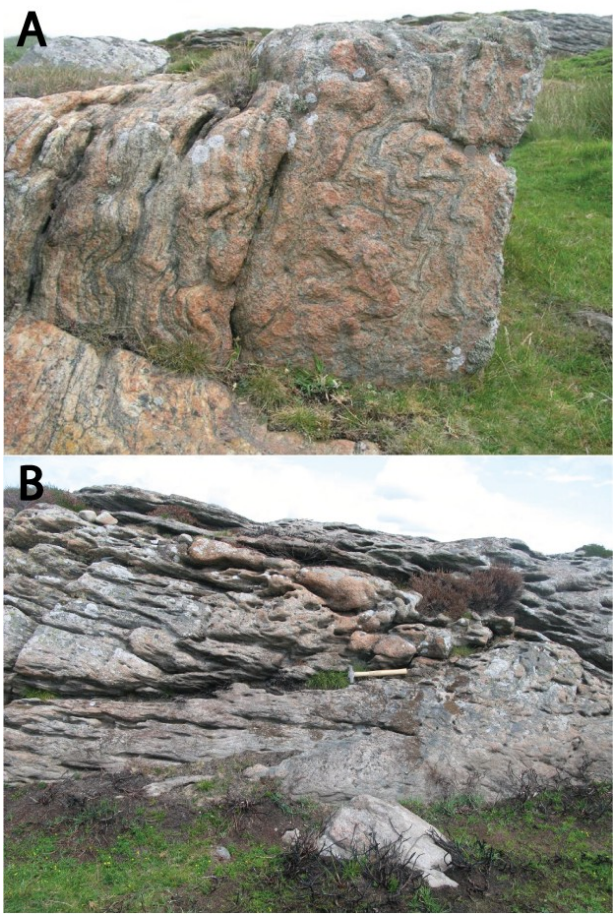


*Fig. 3.* **A.** Migmatite gneiss with red, sugary textured leucosome at Stensjöstrand, host rock for thin sections 3b and 3c. **B.** Migmatite gneiss with sillimanite-rich mesosome at Stensjöstrand. (Photographs by Leif Johansson, Lund University)

# 5 Petrography

Thin section 09SGC-3c has domains that lack sillimanite but are dominated by quartz, plagioclase and K-feldspar (Fig. 4B). Small biotite crystals and opaque minerals also appear in these areas. These opaques have been identified as ilmenite. These domains constitute leucosome, which formed by partial melting of the rock. Small zircon and monazite crystals are present in the leucosome.

Remaining parts of the rock constitute mesosome, rich in sillimanite aggregates with a radiating texture. Along with sillimanite there are also hematite, feldspar, plagioclase, quartz, ilmenite, biotite, garnet, zircon and monazite. Biotite crystals and opaque minerals are scattered and are relatively large (up to 3mm) but have varying shapes. Two biotite crystals were observed with irregular shaped intergrowths of quartz. Textures consisting of worm-like intergrowths (of various minerals) are known as symplectite (Fig. 5A). The opaque minerals were identified as ilmenite and hematite (Fig. 5B). Where present, hematite is associa-

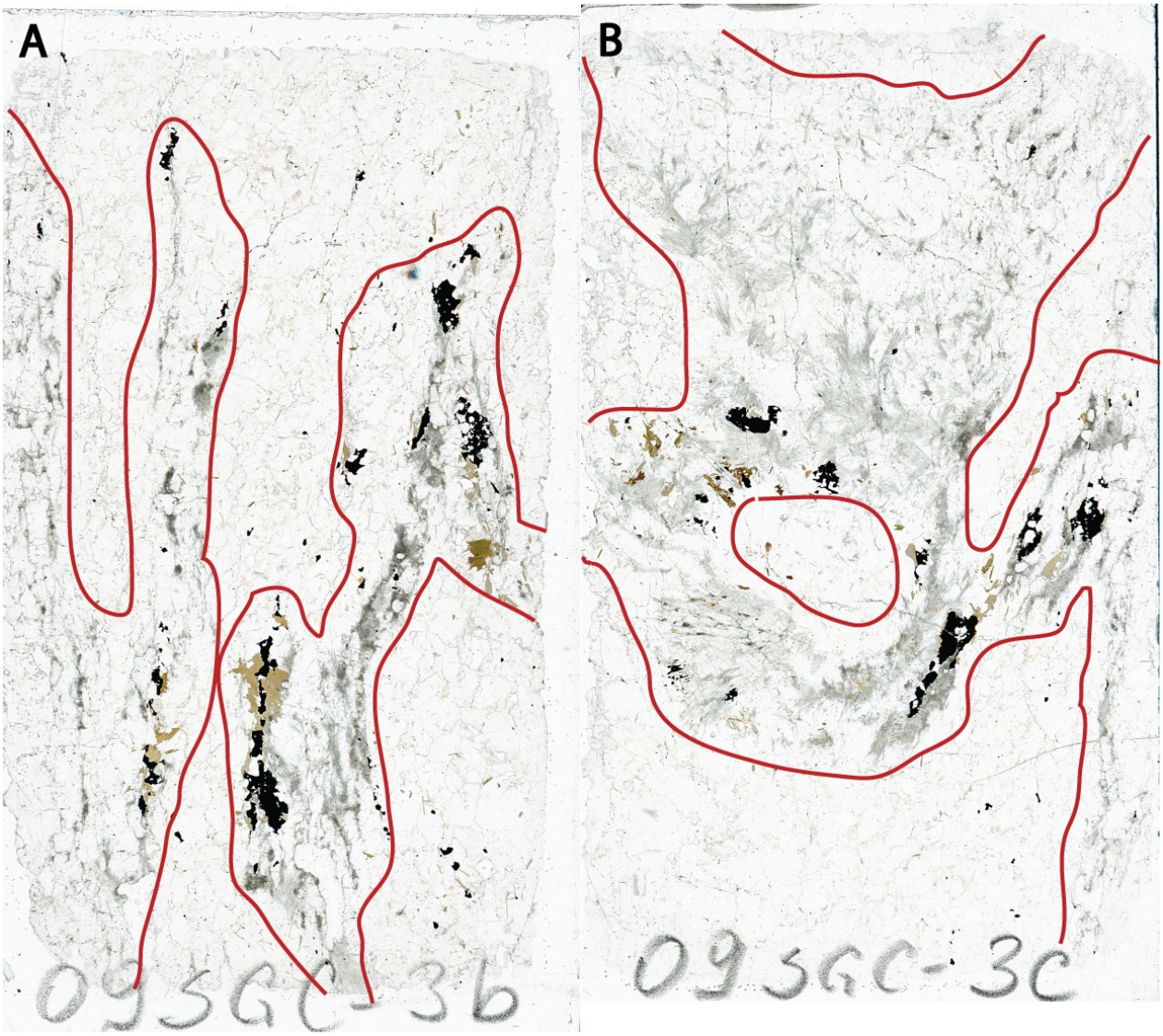


*Fig. 4.* Scanned images of the investigated thin sections. **A.** Thin section 3b. **B.** Thin section 3c. The red lines show the approximate boundaries between the leucosome and the mesosome. The leucosome is characterized by colorless areas, consisting of plagioclase, quartz and K-feldspar with a few small opaque minerals (ilmenite). The mesosome is characterized by sillimanite (grey, radiating), opaques , biotite and garnet.

ted with ilmenite. The ilmenite and feldspar crystals are rich in lamellae (Fig. 5C&D). A few garnet crystals were observed in the thin section.

The monazite crystals in thin section 3c are of two different kinds. The first type is small and oval or round shaped. A BSE image (Fig. 6A) shows one such crystal, compositionally zoned with two different domains, where a darker rim envelops a lighter core. The second type of monazite crystal is typically larger and more irregularly shaped than the first, and has indistinct compositional domains. A BSE image (Fig. 6C) shows one such monazite crystal which has four different domains shown in different shades of grey. Noteworthy is that the different types of monazite crystals appear in different areas of the thin section. The smaller, oval shaped monazite crystals appear almost exclusively in the leucosome whilst the larger irregular shaped monazite crystals appear exclusively in the mesosome.

An as-of-yet unidentified mineral aggregate was found in connection with the larger irregular shaped monazite crystals (Fig. 6E). This type of mineral aggregate occurs as a thin orange coronae that envelopes the monazite crystal. It has at least three shades in BSE, ranging from very bright to dark grey. This mineral aggregate can easily be located through polarization microscopy because of its orange color. It seems to always be associated with both sillimanite and monazite.

A mineral crystal located close by one of the large monazite crystals is most likely fine grained low-grade (retrograde) metamorphic muscovite (Fig. 6F). Similar to the yet unidentified mineral, the muscovite also forms a corona.

Thin section 09SGC-3b (Fig. 4A) has also been studied with a polarization microscope and SEM-EDX. This thin section is from the same rock sample as thin section 3c. Its mineral composition is the same

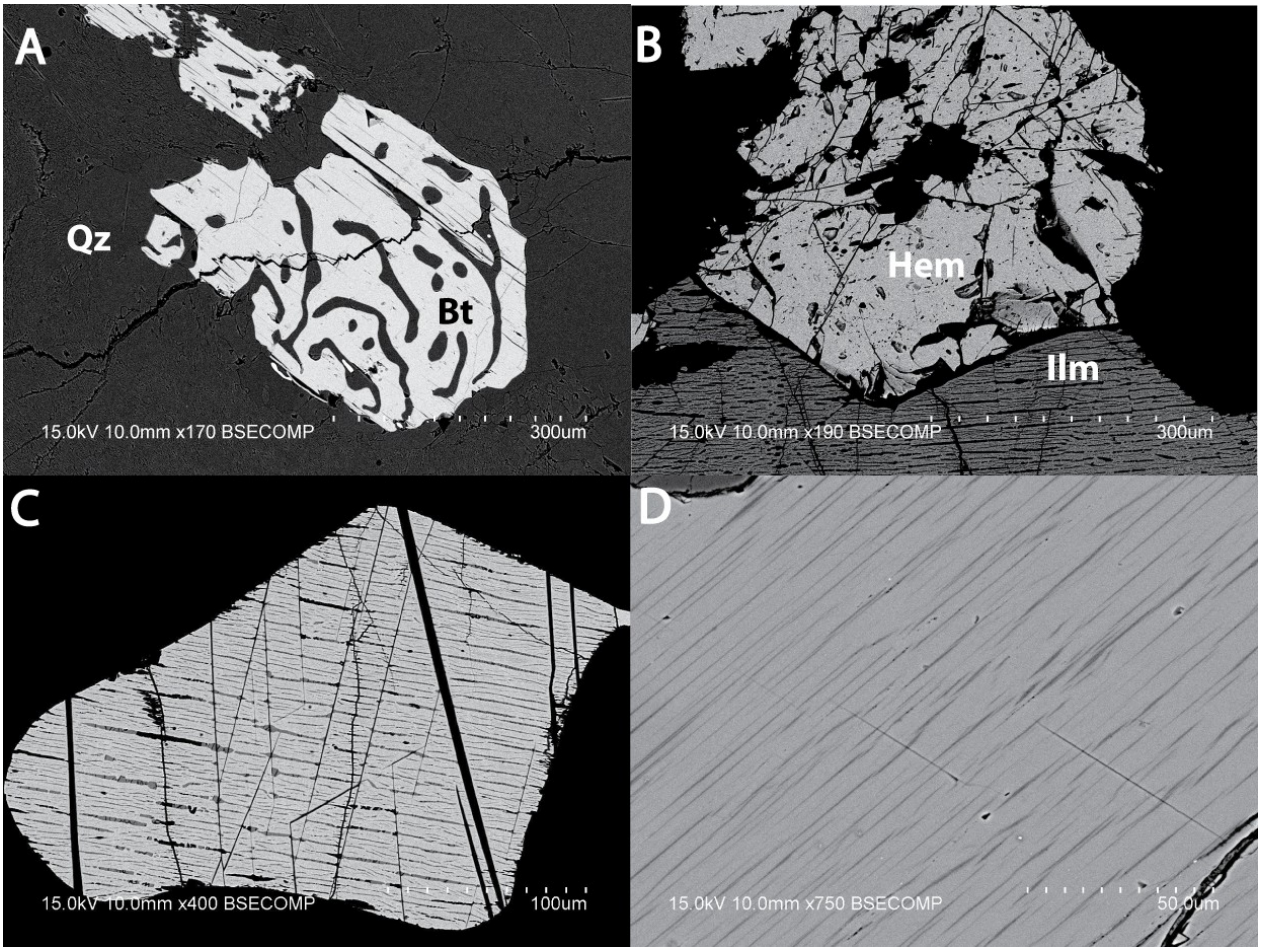


*Fig. 5.* Backscatter electron (BSE) images of different minerals in thin section 3c and lamellae found in both ilmenite and K-feltspar. **A.** Biotite crystal with quartz inclusions (irregular shaped intergrowths also known as symplectite). **B.** Hematite (top) and ilmenite (bottom) in contact. Lamellae are visible in the ilmenite. **C.** Ilmenite crystal with three different kinds of lamellae, identifiable by differences in size and shade. **D.** Thin dark lamellae in K-feldspar identified as albite.

as that of thin section 3c. Akin to thin section 3c, 3b also has leucosome domains which are devoid of sillimanite. Thin section 3b has only a few large, irregular monazite crystals similar to those found in 3c.

## 6 Mineral Chemistry

Tables 1-4 show EDX analyses of the different minerals in thin sections 3b and 3c. Different compositional domains of monazite, varying in shades of grey, were analyzed. Crystal hosts and the respective lamellae of feldspars and ilmenite were analyzed separately.

The analysis results for ilmenite is presented in table 2. The ilmenite crystal hosts has a much greater percentage of Fe than Ti. Three different types of lamellae were observed within the analyzed ilmenite crystals. The first type appears as multiple dark thin lamellae that extend across the ilmenite crystal, lined up from left to right in Fig. 5C. These lamellae had higher Ti values and lower Fe values compared to the crystal host. One of the ilmenite crystals also had Mn in these lamellae. The second type appears as darker spots occurring similarly to the first kind of lamellae but at a smaller extent. These lamellae had much higher Ti values and much lower Fe values than the previous lamellae. The third type appears as large dark cracks that run through the entire crystal, diagonally from top to bottom in Fig. 5C. This type of lamellae was analyzed in ilmenite crystal 2 and akin to the previous lamellae has high amounts of Ti and low amounts of Fe but also trace amounts of Nb.

Regarding the analysis of monazite, many of the wt-% totals deviate greatly from a desirable 100 wt-% total. This is because the available equipment and the setup of mineral standards in the analyzing instrument are not sufficient for analysis of REE and heavy elements such as Y, Yb and Th. As a result of the varying wt-% totals, the information in table 3 is not completely accurate and can only be used for relative comparison between individual monazite crystals. Analysis reveals that all monazite crystals contain Si and most of them also contain Al, although both elements only appear in low amounts. P, Ca, La, Ce and Th occur in varying amounts, some of them have relatively large variations between different mineral crystals. Y, Yb, Nb and S were not found. The results are in some cases not consistent between different monazite crystals and their compositional domains. Si tends to con-

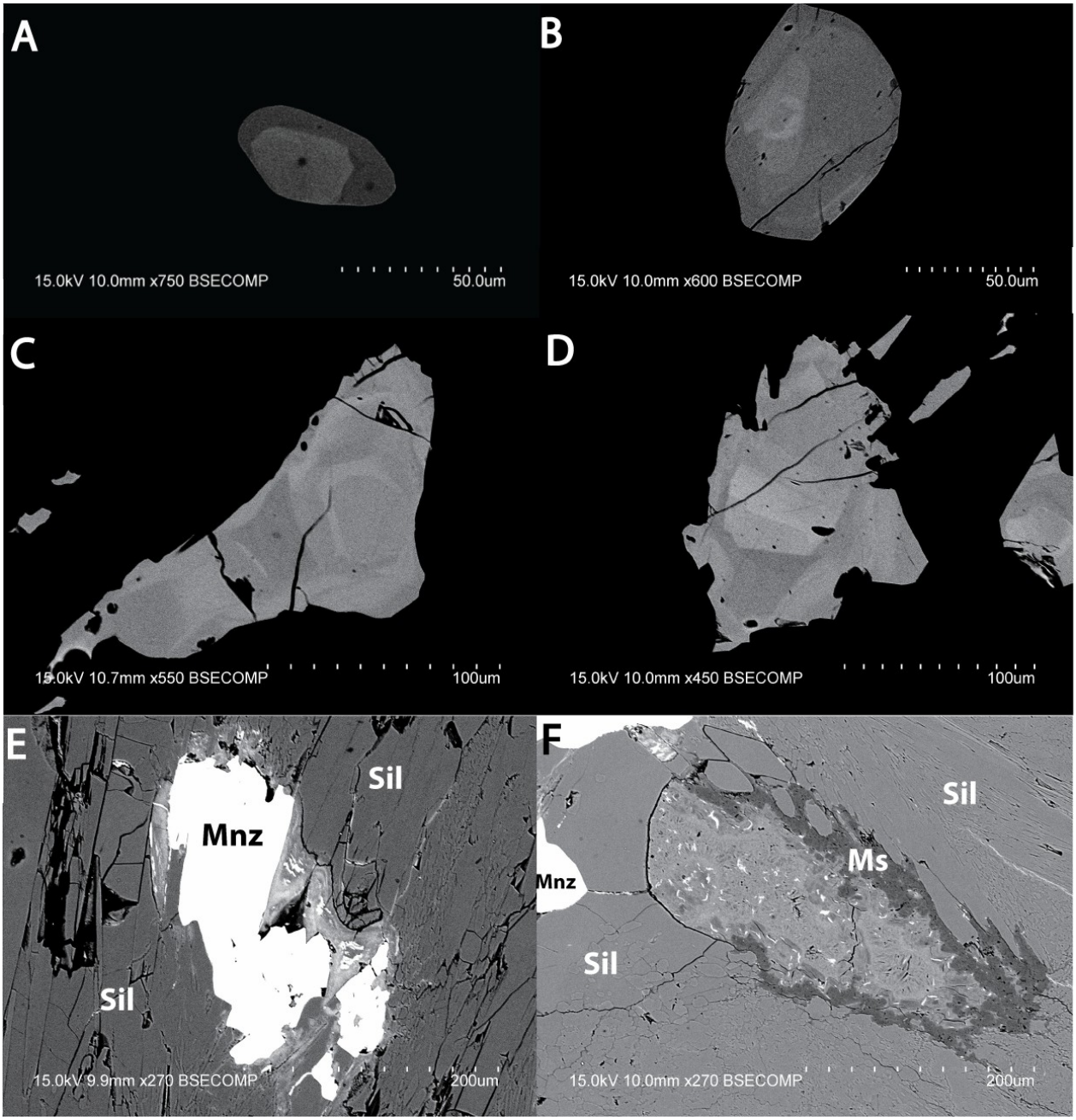


*Fig. 6.* BSE images showing the two types of monazite crystals and complex mineral aggregates found in the mesosome of thin section 3c. **A.** Small monazite with two distinct compositional domains found in the leucosome. The black dots are a result of spot analysis. **B.** Small monazite with several compositional domains found in the leucosome. **C & D.** Large, irregularly shaped monazite crystals with indistinct compositional domains forming complex zoning patterns found in the mesosome. **E.** Monazite with corona of very fine-grained mineral aggregate of unidentified phases located inbetween the monazite crystal and surrounding sillimanite. **F.** Fine-grained, low-grade (retrograde) metamorphic muscovite forming a dark corona around an unidentified mineral aggregate (center) next to a large irregularly shaped monazite crystal (top left).

centrate in lighter domains; an exception to this is small monazite 1. Ca is concentrated in darker domains in large complex monazite 1 & 2 and small monazite 2 whereas the opposite is true for small monazite 1.The results for Ca in large complex monazite 2 are inconsistent. Th tends to be concentrated in lighter domains in all analyzed monazite crystals.

Analysis of K-feldspar and its lamellae reveals that the crystal host has higher K values than Na and the opposite is true for the lamellae (Na>K, table 4). This means that the feldspar in the migmatitic gneiss is perthitic and has an alkali feldspar crystal host with albite lamellae.

The analyzed plagioclase was located in the leucosome; there were no apparent signs of lamellae. The Ca/Na ratios indicate that it is andesine.

*Table. 1.* EDX analyses of minerals in thin section 3b and 3c with the exception of monazite. The majority of the w-t% totals of these analyses are of satisfactory quality.

| | Biotite | Garnet | Hematite | Ilmenite | K-Feldspar | Plagioclase | Quartz | Sillimanite | Zircon |
|---|---|---|---|---|---|---|---|---|---|
| $SiO_2$ | 34.29 | 35.57 | 0 | 0 | 62.65 | 59.69 | 96.69 | 34.79 | 28.96 |
| $TiO_2$ | 2.79 | 0 | 0 | 10.33 | 0 | 0 | 0 | 0 | 0 |
| $Al2O_3$ | 18.1 | 20.85 | 0 | 0 | 18.29 | 24.83 | 0 | 61.35 | 0 |
| MgO | 11.33 | 4.39 | 0 | 0 | 0 | 0 | 0 | 0 | 0 |
| CaO | 0 | 1.75 | 0 | 0 | 0 | 6.38 | 0 | 0 | 0 |
| MnO | 0.44 | 9.48 | 0 | 0 | 0 | 0 | 0 | 0 | 0 |
| FeO | 15.11 | 25.07 | 0 | 78.93 | 0 | 0 | 0 | 0.94 | 0 |
| $Fe_2O_3$ | 0 | 0 | 100.5 | 0 | 0 | 0 | 0 | 0 | 0 |
| $Na_2O$ | 0 | 0 | 0 | 0 | 1.25 | 8.73 | 0 | 0 | 0 |
| $K_2O$ | 9.23 | 0 | 0 | 0 | 14.33 | 0 | 0 | 0 | 0 |
| $ZrO_2$ | 0 | 0 | 0 | 0 | 0 | 0 | 0 | 0 | 70.55 |
| Total w-t% | 91.29 | 97.1 | 100.5 | 89.27 | 96.52 | 99.63 | 96.69 | 97.08 | 99.51 |
| # of oxygen | 10 | 12 | 3 | 3 | 8 | 8 | 2 | 5 | 4 |
| Si | 2.44 | 2.94 | 0 | 0 | 2.98 | 2.67 | 1 | 2 | 0.91 |
| Ti | 0.15 | 0 | 0 | 0.29 | 0 | 0 | 0 | 0 | 0 |
| Al | 1.52 | 2.03 | 0 | 0 | 1.03 | 1.31 | 0 | 9.97 | 0 |
| Mg | 1.2 | 0.54 | 0 | 0 | 0 | 0 | 0 | 0 | 0 |
| Ca | 0 | 0.15 | 0 | 0 | 0 | 0.31 | 0 | 0 | 0 |
| Mn | 0.03 | 0.66 | 0 | 0 | 0 | 0 | 0 | 0 | 0 |
| Fe | 0.9 | 1.73 | 0 | 2.43 | 0 | 0 | 0 | 0.02 | 0 |
| Fe | 0 | 0 | 2 | 0 | 0 | 0 | 0 | 0 | 0 |
| Na | 0 | 0 | 0 | 0 | 0.12 | 0.76 | 0 | 0 | 0 |
| K | 0.84 | 0 | 0 | 0 | 0.87 | 0 | 0 | 0 | 0 |
| Zr | 0 | 0 | 0 | 0 | 0 | 0 | 0 | 0 | 1.09 |
| Cation sum | 7.07 | 8.05 | 2 | 2.71 | 5 | 5.05 | 1 | 3.02 | 2 |

*Table. 2.* EDX analyses of ilmenite and the lamellae found within ilmenite crystals. The Fe-Ti ratios vary greatly between the crystal host and the different lamellae. The ”light” and ”dark” affixes describe which compound domain has been analyzed.

| | Ilmenite 1 | | | Ilmenite 2 | | | |
|---|---|---|---|---|---|---|---|
| | Crystal host | Light lamellae | Dark lamellae | Crystal host | Light lamellae | Dark lamellae | Dark crack |
| $Al_2O_3$ | 0 | 0 | 0 | 0 | 0.7 | 29.59 | 0 |
| $SiO_2$ | 0 | 0 | 0 | 0 | 0.44 | 0 | 0 |
| $TiO_2$ | 10.33 | 49.9 | 87.69 | 10.34 | 20.6 | 52.64 | 90.88 |
| MnO | 0 | 4.71 | 0 | 0 | 0 | 0 | 0 |
| FeO | 78.93 | 44.07 | 10.66 | 74.05 | 64.96 | 7.94 | 2.43 |
| $Nb_2O_5$ | 0 | 0 | 0 | 0 | 0 | 0 | 2.6 |
| Total w-t% | 89.27 | 98.68 | 98.35 | 84.39 | 86.7 | 90.17 | 95.91 |
| Formula based on 3 oxygen | | | | | | | |
| Al | 0 | 0 | 0 | 0 | 0.03 | 0.76 | 0 |
| Si | 0 | 0 | 0 | 0 | 0.01 | 0 | 0 |
| Ti | 0.29 | 0.97 | 1.41 | 0.3 | 0.53 | 0.86 | 1.45 |
| Mn | 0 | 0.1 | 0 | 0 | 0 | 0 | 0 |
| Fe | 2.43 | 0.95 | 0.19 | 2.4 | 1.86 | 0.14 | 0.04 |
| Nb | 0 | 0 | 0 | 0 | 0 | 0 | 0.02 |
| Cation sum | 2.71 | 2.03 | 1.6 | 2.7 | 2.44 | 1.76 | 1.52 |

*Table. 3.* EDX analyses of monazite crystals in mesosome and leucosome. The ”light” and ”dark” affixes describe which compound domain has been analyzed. The top half of the table shows values for large complex monazites found in the mesosome. The bottom half shows values for small monazites found in the leucosome. The results for ”large complex monazite 2” are erroneous.

Large complex monazites

| | 1 | | | | | 2 | | | | 3 |
|---|---|---|---|---|---|---|---|---|---|---|
| | Darkest | Second Darkest | Intermetiade Shade | Second Lightest | Lightest | Darkest | Second Darkest | Second Lightest | Lightest | Random Spot |
| $Al_2O_3$ | 0.4 | 0.28 | 0.42 | 0.45 | 0.5 | 0.88 | 0.44 | 0.29 | 1.17 | 0 |
| $SiO_2$ | 0.34 | 0.74 | 0.72 | 1.56 | 1.34 | 1.04 | 0.88 | 1.11 | 2.14 | 0.71 |
| $P_2O_5$ | 27.59 | 27.65 | 28.61 | 27.9 | 26.71 | 45.97 | 26.95 | 26.94 | 25.18 | 26.53 |
| CaO | 2.36 | 1.91 | 1.12 | 1 | 0.57 | 3.28 | 0.97 | 1.43 | 1.08 | 1.01 |
| $La_2O_3$ | 13.84 | 14.43 | 14.17 | 13.39 | 13.84 | 24.38 | 13.44 | 11.68 | 11.73 | 13.25 |
| $Ce_2O_3$ | 30.86 | 31.84 | 32.54 | 32.69 | 32.57 | 53.32 | 30.78 | 28.39 | 27.8 | 31.28 |
| $ThO_2$ | 5.62 | 5.32 | 4.45 | 6.54 | 6.66 | 10.11 | 4.2 | 6.69 | 4.66 | 4.68 |
| Total w-t% | 81.01 | 82.17 | 82.04 | 83.53 | 82.18 | 138.98 | 77.66 | 76.53 | 73.76 | 77.46 |
| Formula based on 4 oxygen | | | | | | | | | | |
| Al | 0.02 | 0.01 | 0.02 | 0.02 | 0.03 | 0.03 | 0.02 | 0.02 | 0.07 | 0 |
| Si | 0.02 | 0.03 | 0.03 | 0.07 | 0.06 | 0.03 | 0.04 | 0.05 | 0.1 | 0.03 |
| P | 1.04 | 1.04 | 1.06 | 1.02 | 1.01 | 1.03 | 1.05 | 1.06 | 1.01 | 1.05 |
| Ca | 0.11 | 0.09 | 0.05 | 0.05 | 0.03 | 0.09 | 0.05 | 0.07 | 0.05 | 0.05 |
| La | 0.23 | 0.24 | 0.23 | 0.21 | 0.23 | 0.24 | 0.23 | 0.2 | 0.2 | 0.23 |
| Ce | 0.51 | 0.52 | 0.52 | 0.52 | 0.53 | 0.51 | 0.52 | 0.48 | 0.48 | 0.54 |
| Th | 0.06 | 0.05 | 0.04 | 0.06 | 0.07 | 0.06 | 0.04 | 0.07 | 0.05 | 0.05 |
| Cation sum | 1.98 | 1.98 | 1.95 | 1.96 | 1.96 | 1.98 | 1.95 | 1.95 | 1.96 | 1.95 |

Small monazites in leucosome

| | 1 | | | 2 | | 3 |
|---|---|---|---|---|---|---|
| | Darkest | Intermediate Shade | Lightest | Darkest | Lightest | Random Spot |
| $Al_2O_3$ | 0 | 0.54 | 0 | 0 | 0 | 0 |
| $SiO_2$ | 1.19 | 1.35 | 1.17 | 0.66 | 1.1 | 0.82 |
| $P_2O_5$ | 26.47 | 27.01 | 27.02 | 29.22 | 28.89 | 27.19 |
| CaO | 1.38 | 1 | 1.98 | 1.89 | 1.03 | 1.16 |
| $La_2O_3$ | 12.14 | 14.45 | 11.68 | 14.25 | 12.97 | 13.55 |
| $Ce_2O3$ | 31.91 | 30.3 | 33.92 | 32.83 | 32.56 | 31.07 |
| $ThO_2$ | 5.71 | 6.42 | 11.2 | 5.43 | 5.77 | 4.17 |
| Total w-t% | 78.82 | 81.07 | 86.97 | 84.29 | 82.31 | 77.95 |
| Formula based on 4 oxygen | | | | | | |
| Al | 0 | 0.03 | 0 | 0 | 0 | 0 |
| Si | 0.06 | 0.06 | 0.05 | 0.03 | 0.05 | 0.04 |
| P | 1.03 | 1.02 | 1 | 1.06 | 1.06 | 1.06 |
| Ca | 0.07 | 0.05 | 0.09 | 0.09 | 0.05 | 0.06 |
| La | 0.21 | 0.24 | 0.19 | 0.22 | 0.21 | 0.23 |
| Ce | 0.54 | 0.5 | 0.54 | 0.51 | 0.52 | 0.52 |
| Th | 0.06 | 0.07 | 0.11 | 0.05 | 0.06 | 0.04 |
| Cation sum | 1.96 | 1.96 | 1.98 | 1.96 | 1.94 | 1.95 |

*Table. 4.* Feldspar analyses showing the difference in Na and K between the crystal host and the lamellae.

| | K-Feldspar | Lamellae |
|---|---|---|
| $Na_2O$ | 1.25 | 10.97 |
| $Al_2O_3$ | 18.29 | 19.31 |
| $SiO_2$ | 62.65 | 65.47 |
| $K_2O$ | 14.33 | 1.43 |
| Total w-t% | 96.52 | 97.17 |
| | | |
| Formula based on 5 oxygen | | |
| Na | 0.96 | 0.12 |
| Al | 1.03 | 1.03 |
| Si | 2.97 | 2.98 |
| K | 0.08 | 0.87 |
| Cation sum | 5.04 | 5 |

# 7 Interpretation and Discussion

The occurrence of lamellae in both ilmenite and feldspar is a result of exsolution. The short explanation of exsolution is that different components in a mineral crystal unmix and separate when pressure and/or temperature conditions change. If this happens to a high-temperature alkali feldspar crystal then Na-rich and K-rich segregations will unmix. Depending on whether the feldspar is perthite (K-rich) or antiperthite (Na-rich) the least abundant component of the feldspar will form lamellae (Winter, 2010).

Monazite crystals in thin section 3b and 3c have two different appearances. The first type is smaller, round or oval shaped and appears almost exclusively in the leucosome. The second type of monazite is large, has irregular crystal shapes and appears exclusively in the mesosome. It can be said that the monazite in the mesosome is older than the monazite in the leucosome, because the mesosome must have existed before it was partially melted. The age difference could explain the textures of the two types of monazite crystals. The older monazites have experienced longer periods of metamorphism which have resulted in several growth zones in the crystals. The younger monazites have not experienced as much metamorphic activity which could explain their shape, small size and distinct compositional domains.

The textures (rounded corners, sharp edges and embayments) of the large monazite crystals in the mesosome look like resorption textures. Resorption occurs due to mineral dissolution, as a response to changing metamorphic conditions (Winter, 2010).

The presence of the large, complex type monazite coincides with the presence of garnet in the mesosome. Monazite and garnet are both sinks for Y and comparing the concentration between the two minerals can give insight into which order they crystallized (Williams et al., 2007). This connection has not been able to be confirmed in this study because the analyzing equipment could not detect Y.

The relative differences in chemical compositions of the analyzed monazite crystal are difficult to interpret without access to a WDS-instrument which has a higher spectral resolution and sensitivity than EDS. The low contents of trace elements and the overlapping peaks of heavy elements including REE renders EDX analyses of monazite difficult. Thus the differences in composition between the studied monazite crystals and domains cannot be fully assessed.

The only consistency between the analyzed monazite crystals was the differences in Th concentrations; Th tends to concentrate in the lighter domains. Perhaps this was the cause for the different shades in the BSE-images.

# 8 Conclusions

There is a clear difference in mineral texture and mineral assemblage between the leucosome and the mesosome which is a result from partial melting.

The exsolution and resorption textures in the ilmenite, feldspar and monazite crystals respectively indicate changing physical conditions in the host rock over time.

Two types of monazite crystals have been observed, each is strictly limited to either the leucosome or the mesosome.

The difference in texture between the monazite crystals indicate they have experienced different metamorphic events meaning that they have not formed at the same time.

# 9 Follow-up

To follow-up on this study there are a few suggestions.

Further study of some of the other minerals, such as the exsoluted ilmenite and feldspar or garnet and hematite crystals, and their connection to the leucosome and mesosome could perhaps prove to be a viable way to give insight into the metamorphic history of the metasediment.

The monazite in the metasediment could be analyzed with more powerful analytic instruments so that the metamorphic history of the metasediments in Stensjöstrand can be examined more effectively. The mineral could also be used for dating of the rock.

An interesting question that still remains without a certain answer from this study is the cause of the differences between the two types of monazite that appear in the leucosome and the mesosome.

# 10 Acknowledgements

I want to thank my supervisor, Charlotte Möller, and my secondary supervisor, Leif Johansson, for their help and support during the course of this study. I would also like to thank Anna Eklöv Pettersson for our insightful discussions and conversations on the subject which have been of great help.

# 11 References


BGS, B. G. S. 2011. Rare Earth Elements Profile. 54.

Boatner, L. A. 2002. Synthesis, structure, and properties of monazite, pretulite, and xenotime. Reviews in Mineralogy and Geochemistry, 48, 87-121.

Dean, S., Pinan-Llamas, A., Johansson, L., Reimink, J. & Hansen, E. 2008. Deformation and migmatization in the Stensjostrands Naturreservat, Halland Province, SW Sweden. Abstracts with Programs - Geological Society of America, 40, 146.

Deer, W. A., Howie, R. A. & Zussman, J. 1962. Rock-forming minerals; vol. 5, Non- silicates. 371.

J. Andersson & C. Möller. Unpublished.

Spear, F. S. & Pyle, J. M. 2002. Apatite, monazite, and xenotime in metamorphic rocks. Reviews in Mineralogy and Geochemistry, 48, 293-335.

Williams, M. L., Jercinovic, M. J. & Hetherington, C. J. 2007. Microprobe monazite geochronology; understanding geologic processes by integrating composition and chronology. Annual Review of Earth and Planetary Sciences, 35, 137-175.

Winter, J. D. 2010. An introduction to igneous and metamorphic petrology / John D. Winter, New York : Prentice Hall, cop. 2010, 2. ed., International ed.

**Tidigare skrifter i serien ”Examensarbeten i Geologi vid Lunds universitet”:**

309. Leskelä, Jari, 2012: Loggning och återfyllning av borrhål – Praktiska försök och utveckling av täthetskontroll i fält. (15 hp)
310. Eriksson, Magnus, 2012: Stratigraphy, facies and depositional history of the Colonus Shale Trough, Skåne, southern Sweden. (45 hp)
311. Larsson, Amie, 2012: Kartläggning, beskrivning och analys av Kalmar läns regionalt viktiga vattenresurser. (15 hp)
312. Olsson, Håkan, 2012: Prediction of the degree of thermal breakdown of limestone: A case study of the Upper Ordovician Boda Limestone, Siljan district, central Sweden. (45 hp)
313. Kampmann, Tobias Christoph, 2012: U-Pb geochronology and paleomagnetism of the Westerberg sill, Kaapvaal Craton – support for a coherent Kaapvaal-Pilbara block (Vaalbara). (45 hp)
314. Eliasson, Isabelle Timms, 2012: Arsenik: förekomst, miljö och hälsoeffekter. (15 hp)
315. Badawy, Ahmed Salah, 2012: Sequence stratigraphy, palynology and biostratigraphy across the Ordovician-Silurian boundary in the Röstånga-1 core, southern Sweden. (45 hp)
316. Knut, Anna, 2012: Resistivitets- och IP-mätningar på Flishultsdeponin för lokalisering av grundvattenytor. (15 hp)
317. Nylén, Fredrik, 2012: Förädling av ballastmaterial med hydrocyklon, ett fungerande alternativ? (15 hp)
318. Younes, Hani, 2012: Carbon isotope chemostratigraphy of the Late Silurian Lau Event, Gotland, Sweden. (45 hp)
319. Weibull, David, 2012: Subsurface geological setting in the Skagerrak area – suitability for storage of carbon dioxide. (15 hp)
320. Petersson, Albin, 2012: Förutsättningar för geoenergi till idrottsanläggningar i Kallerstad, Linköpings kommun: En förstudie. (15 hp)
321. Axbom, Jonna, 2012: Klimatets och människans inverkan på tallens etablering på sydsvenska mossar under de senaste århundradena – en dendrokronologisk och torvstratigrafisk analys av tre småländska mossar. (15 hp)
322. Kumar, Pardeep, 2012: Palynological investigation of coal-bearing deposits of the Thar Coal Field Sindh, Pakistan. (45 hp)
323. Gabrielsson, Johan, 2012: Havsisen i arktiska bassängen – nutid och framtid i ett globalt uppvärmningsperspektiv. (15 hp)
324. Lundgren, Linda, 2012: Variation in rock quality between metamorphic domains in the lower levels of the Eastern Segment, Sveconorwegian Province. (45 hp)
325. Härling, Jesper, 2012: The fossil wonders of the Silurian Eramosa Lagerstätte of Canada: the jawed polychaete faunas. (15 hp)
326. Qvarnström, Martin, 2012: An interpretation of oncoid mass-occurrence during the Late Silurian Lau Event, Gotland, Sweden. (15 hp)
327. Ulmius, Jan, 2013: P-T evolution of paragneisses and amphibolites from Romeleåsen, Scania, southernmost Sweden. (45 hp)
328. Hultin Eriksson, Elin, 2013: Resistivitetsmätningar för avgränsning av lakvattenplym från Kejsarkullens deponis infiltrationsområde. (15 hp)
329. Mozafari Amiri, Nasim, 2013: Field relations, petrography and 40Ar/39Ar cooling ages of hornblende in a part of the eclogite-bearing domain, Sveconorwegian Orogen. (45 hp)
330. Saeed, Muhammad, 2013: Sedimentology and palynofacies analysis of Jurassic rocks Eriksdal, Skåne, Sweden. (45 hp)
331. Khan, Mansoor, 2013: Relation between sediment flux variation and land use patterns along the Swedish Baltic Sea coast. (45 hp)
332. Bernhardson, Martin, 2013: Ice advance-retreat sediment successions along the Logata River, Taymyr Peninsula, Arctic Siberia. (45 hp)
333. Shrestha, Rajendra, 2013: Optically Stimulated Luminescence (OSL) dating of aeolian sediments of Skåne, south Sweden. (45 hp)
334. Fullerton, Wayne, 2013: The Kalgoorlie Gold: A review of factors of formation for a giant gold deposit. (15 hp)
335. Hansson, Anton, 2013: A dendroclimatic study at Store Mosse, South Sweden – climatic and hydrologic impacts on recent Scots Pine (*Pinus sylvestris*) growth dynamics. (45 hp)
336. Nilsson, Lawrence, 2013: The alteration

mineralogy of Svartliden, Sweden. (30 hp)

337. Bou-Rabee, Donna, 2013: Investigations of a stalactite from Al Hota cave in Oman and its implications for palaeoclimatic reconstructions. (45 hp)
338. Florén, Sara, 2013: Geologisk guide till Söderåsen – 17 geologiskt intressanta platser att besöka. (15 hp)
339. Kullberg, Sara, 2013: Asbestkontamination av dricksvatten och associerade risker. (15 hp)
340. Kihlén, Robin, 2013: Geofysiska resistivitetsmätingar i Sjöcrona Park, Helsingborg, undersökning av områdets geologiska egenskaper samt 3D modellering i GeoScene3D. (15 hp)
341. Linders, Wictor, 2013: Geofysiska IP-undersökningar och 3D-modellering av geofysiska samt geotekniska resultat i GeoScene3D, Sjöcrona Park, Helsingborg, Sverige. (15 hp)
342. Sidenmark, Jessica, 2013: A reconnaissance study of Rävliden VHMS-deposit, northern Sweden. (15 hp)
343. Adamsson, Linda, 2013: Peat stratigraphical study of hydrological conditions at Stass Mosse, southern Sweden, and the relation to Holocene bog-pine growth. (45 hp)
344. Gunterberg, Linnéa, 2013: Oil occurrences in crystalline basement rocks, southern Norway – comparison with deeply weathered basement rocks in southern Sweden. (15 hp)
345. Peterffy, Olof, 2013: Evidence of epibenthic microbial mats in Early Jurassic (Sinemurian) tidal deposits, Kulla Gunnarstorp, southern Sweden. (15 hp)
346. Sigeman, Hanna, 2013: Early life and its implications for astrobiology – a case study from Bitter Springs Chert, Australia. (15 hp)
347. Glommé, Alexandra, 2013: Texturella studier och analyser av baddeleyitomvandlingar i zirkon, exempel från sydöstra Ghana. (15 hp)
348. Brådenmark, Niklas, 2013: Alunskiffer på Öland – stratigrafi, utbredning, mäktigheter samt kemiska och fysikaliska egenskaper. (15 hp)
349. Jalnefur Andersson, Evelina, 2013: En MIFO fas 1-inventering av fyra potentiellt förorenade områden i Jönköpings län. (15 hp)
350. Eklöv Pettersson, Anna, 2013: Monazit i Obbhult-komplexet: en pilotstudie. (15 hp)
351. Acevedo Suez, Fernando, 2013: The reliability of the first generation infrared refractometers. (15 hp)
352. Murase, Takemi, 2013: Närkes alunskiffer – utbredning, beskaffenhet och oljeinnehåll. (15 hp)
353. Sjöstedt, Tony, 2013: Geoenergi – utvärdering baserad på ekonomiska och drifttekniska resultat av ett passivt geoenergisystem med värmeuttag ur berg i bostadsrättsföreningen Mandolinen i Lund. (15 hp)
354. Sigfúsdóttir, Thorbjörg, 2013: A sedimentological and stratigraphical study of Veiki moraine in northernmost Sweden. (45 hp)
355. Månsson, Anna, 2013: Hydrogeologisk kartering av Hultan, Sjöbo kommun. (15 hp)
356. Larsson, Emilie, 2013: Identifying the Cretaceous–Paleogene boundary in North Dakota, USA, using portable XRF. (15 hp)
357. Anagnostakis, Stavros, 2013: Upper Cretaceous coprolites from the Münster Basin (northwestern Germany) – a glimpse into the diet of extinct animals. (45 hp)
358. Olsson, Andreas, 2013: Monazite in metasediments from Stensjöstrand: A pilot study. (15 hp)


LUNDS UNIVERSITET

Geologiska institutionen
Lunds universitet
Sölvegatan 12, 223 62 Lund